Optik - International Journal for Light and Electron Optics 206 (2020) 164266

Contents lists available at ScienceDirect

Optik

journal homepage: www.elsevier.com/locate/ijleo

Original research article

Maximum emission levels of photonically generated impulse radio waveforms under spectral constraints

Mohamed Shehata[a], Abdelrhman M. Abotaleb[a], Moaz G. Ali[b], Mohamed Farhat O. Hameed[c,d], Hassan Mostafa[e,f,*], Salah S.A. Obayya[g,h]

[a] The Department of Electronics and Electrical Communications Engineering, Cairo University, Giza 12613, Egypt
[b] Physics of Earth and Universe Department, University of Science and Technology, Zewail City of Science and Technology, October Gardens, Giza 12578, Egypt
[c] The Centre for Photonics and Smart Materials, and Nanotechnology Engineering Program, Zewail City of Science and Technology, Giza 12578, Egypt
[d] The Department of Mathematics and Engineering Physics, Faculty of Engineering, Mansoura University, Mansoura 35516, Egypt
[e] University of Science and technology, Nanotechnology and Nanoelectronics Program , Zewail City of Science and Technology, October Gardens, 6th of October, Giza 12578, Egypt
[f] Department of Electrical Engineering, Cairo University, Giza 12613, Egypt
[g] The Centre for Photonics and Smart Materials, Zewail City of Science and Technology, Giza 12578, Egypt
[h] The Department of Electronics and communication Engineering Department, Faculty of Engineering, Mansoura University, Mansoura 35516, Egypt

ARTICLE INFO

Keywords:
FCC
PSD
IR-UWB
ESD

ABSTRACT

Since it has been first discovered in the analysis of the black-body radiation problem, the emission of spectrally constrained electromagnetic radiation is frequently encountered at different parts of the spectrum, ranging from microwave (MW) frequencies, up to the visible band of the spectrum. These spectral constraints tend to limit the radiated electromagnetic energy, its spectral density and/or the bandwidth occupied by this energy. In this work, analytical closed-form expressions are developed for the maximum emission levels of photonically generated impulse radio-ultrawide band (IR-UWB) waveforms. Both the energy spectral density (ESD) and the bandwidth constraints imposed on these waveforms are considered. The validity of using the derived expressions as upper bounds on the radiation efficiencies of IR-UWB waveforms in practical UWB systems is experimentally demonstrated. Although the conducted analysis is applied to the MW band, it has the advantage of being applicable to other impulse waveforms that occupy other parts of the electromagnetic spectrum, including the milli-meter wave band and the tera-Hertz band, under arbitrarily different ESD and bandwidth constraints.

1. Introduction

Numerous optical pulse shaping techniques have been employed to generate pulsed electromagnetic radiation at different bands below the visible band of the spectrum, such as the microwave (MW) band [1–3], the milli-meter wave (MMW) band [4–6] or the tera-Hertz (THz) band [7,8]. Among these technologies, the ultra-wide band (UWB) lies within the most appropriate techniques

* Corresponding author at: The Nanotechnolgy Engineering Program, University of Science and Technology, Zewail City of Science and Technology, October Gardens, Giza 12578, Egypt.
E-mail addresses: m.shehata_ieee@yahoo.com (M. Shehata), profvip.abotaleb@gmail.com (A.M. Abotaleb), s-moaaz.mohamed@zewailcity.edu.eg (M.G. Ali), mfarahat@zewailcity.edu.eg (M.F. O. Hameed), hmostafa@zewailcity.edu.eg (H. Mostafa), sobayya@zewailcity.edu.eg (S.S.A. Obayya).

https://doi.org/10.1016/j.ijleo.2020.164266
Received 6 December 2019; Accepted 19 January 2020

chosen for many high data rate and short range wireless applications. However, UWB signal transmission requires very low power to obey the FCC regulations reaches as low as 560 μW [1]. Moreover the power of a radiated UWB signal is inevitably reduced by the frequency-dependent transmission loss offered by the UWB wireless link, including the spectrum of both the transmitting and receiving UWB antennas. Therefore, the available energy for an UWB waveform should be efficiently utilized such that the minimum power requirements (above the sensitivity threshold) are secured at the UWB receiver front end. Different techniques have been developed with the aim of optimizing the radiated energy and the received energy of the UWB signals. For instance, in [2], closed-form expressions have been developed to estimate the link energy loss in UWB systems as a ratio of the received UWB waveform energy to its transmitted energy. However, the analysis provided in [2] is limited to only Gaussian and Gaussian monocycle excitation waveforms radiated by specific transmit and receive antenna types such as the electrically small dipole and loop antennas. It should be highlighted that, more recently, other Gaussian-based UWB waveforms, such as doublets, triplets and higher order derivatives [3], have also been widely adopted for UWB signalling. In addition, UWB waveforms have been derived from basis functions that possess non-Gaussian profiles, such as the hyperbolic secant (sech) pulse [4].

In [5], an analytical approach has been proposed to maximize the received voltage amplitude, for bandlimited signals, at the output of the receive antenna, with an inequality constraint on the energy delivered to the transmit antenna. These constraints have been imposed on the total UWB waveform energy admissible by the FCC. However, restricting the total energy of an UWB waveform does not necessarily guarantee that its PSD achieves either partial or full obeying of the FCC regulations of a spectrum masking restrictions, especially in the 3.1–10.6 GHz band. In [6], closed form analytical expressions of the optimum electric fields of signals emitted by an arbitrary shape UWB antenna have been presented, with the objective criterion includes either for a specific position and time maximizing the electric field, or for a location where over a pre-specified time range maximizing the energy spatial density. Although comprehensive, the analysis presented in [6] has been applied to a very specific case of UWB antenna-waveform combination. In particular, the amplitude of the electric field radiated by a 15 cm wire dipole antenna has been optimized, considering a Gaussian doublet pulse whose temporal width is selected to obtain a signal with most of its energy s intensified around the spectrum range 100–2000 MHz. In this work, accurate analytical formula for the upper bounds of the radiation efficiencies (REs) of photonically produced IR-UWB signals are developed, considering the FCC regulations for the spectrum used. The validity of using the developed formulas as upper limit of the RE in practical UWB systems is experimentally verified. A UWB antenna is designed and fabricated, and its spectral and spatial radiation characteristics are experimentally measured. The impact of transmitting typical IR-UWB waveforms on a realistic UWB medium, including the frequency response of the fabricated UWB antenna, on the REs of the considered waveforms is evaluated after wireless transmission [9].

2. Spectral radiation efficiency of emitted IR-UWB waveforms

Fig. 1 illustrates a typical block diagram that overviews the general concept of the photonic generation of pulsed electromagnetic radiation in the sub-visible band via optical pulse shaping. As clear from this figure, one or more optical sources excites a photonic processing stage, where various optical phenomena are usually used to reshape the frequency response of the exciting optical signal. The field-matter interaction dynamics utilized to reshape the optical spectrum depends on the particular material(s) that form this stage as well as its geometrical structure [10]. The processed optical waveform is then down-converted to the sub-visible wavelength domain by using a high-speed photo-detector (PD). The photo-detected energy is then electrically processed before being radiated to the free space via a transmit antenna. A receiving antenna, positioned at a distance L m from the transmit antenna, collects the propagating energy, which is then forwarded to further electrical processing. In this context, the system in Fig. 1 is assumed to generate IR-UWB waveform in the MW band. As in [2,5], to maximize the transmitted energy and the received energy of an UWB waveform, it is assumed that the source impedance $Z_G(\omega) = 0$ and the load impedance $Z_L(\omega) \rightarrow \infty$. The RE of a UWB waveform is calculated before and after wireless transmission, corresponding to Points B and C in Fig. 1, respectively.

Most often, photonically generated IR-UWB signals are derivatives with magnitude and/or time scaling of a typical optical gaussian pulse or a sech pulse. The optical excitation basis function (at Point A in Fig. 1), designated as $\psi\left(\frac{t}{\tau}\right)$, which is defined as follows:

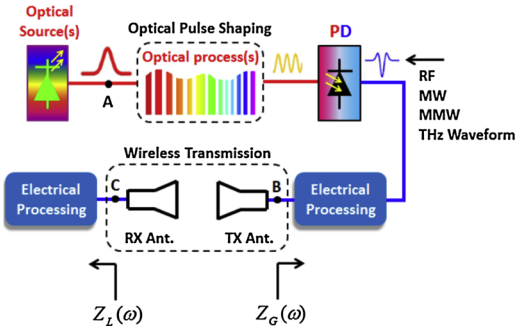

Fig. 1. Circuit schematic/block diagram representation of a typical UWB communications chain.

$$\Psi\left(\frac{t}{\tau}\right)_{-\infty\le t\le\infty} = \begin{cases}\exp(-t^2/\tau_g^2) & \text{gaussian pulse case}\\ \operatorname{sech}(t/\tau_s); & \text{sech pulse case}\end{cases} \tag{1}$$

where τ_g is the Gaussian pulse width, τ_s is the sech pulse width and τ is the full width at half maximum (FWHM) pulse width of both pulse types, which is expanded to express either the gaussian or sech pulse widths as $\tau = 2\sqrt{-\log\left(\frac{1}{2}\right)}\tau_g$ in case of guassian pulse, and $\tau = 2\,\mathrm{sech}^{-1}(1/2)\tau_s$ in case of sech pulse [11]. The Fourier transform of the *mth* order derivative of (1), normalized to the FCC spectral mask, is represented as shown in Eq. (2)[9].

$$\begin{aligned}\Psi^{(k)}_{n,\text{normalized}}(j\omega,\tau) &= A_n(j\omega)^k\Im\{\psi(t/\tau)\}\\ &= A_n\begin{cases}(j\omega)^k\tau_g\sqrt{\pi}\exp\left(\dfrac{-(\omega\tau_g)^2}{2}\right)\\ (j\omega)^k 4{*}\pi\tau_s\operatorname{sech}(2\pi\omega\tau_s)\end{cases}\end{aligned} \tag{2}$$

where $\psi^{(k)}_{n,\text{normalized}}(j\omega;\tau)$ denotes the Fourier transform done over the kth derivative of the basis signal $\psi(t/\tau)$, normalized to the maximum admissible FCC PSD, $\zeta\{.\}$ denotes the Fourier transform operation and A_n is given by:

$$A_n = \left(\frac{\max\{S_{\text{mask}}(\omega)\}}{\max\{|(j\omega)^k\zeta\{\psi(t/\tau)\}|^2\}}\right) \tag{3}$$

where $S_{mask}(\omega)$ denotes the FCC regulation mask in the frequency domain. It should be noted that, A_n is a normalization constant that scales the maximum value of the power spectral density of the kth derivative of IR-UWB signal to be a peak obeying the constraints by FCC regulation mask in the frequency domain.

The efficiency of UWB radiation is usually measured by calculating the radiation efficiency of the transmitting and receiving UWB waveform. According to [3], the RE of a UWB signal is described as the fraction useful in UWB from the power spectral density to the total power under the FCC regulations curve, and is given by

$$\eta = \frac{\int_\Omega |\psi^{(k)}_{n,\text{normalized}}(j\omega,\tau)|^2|H_{\text{norm}}(j\omega)|^2 d\omega}{\int_\Omega S_{\text{mask}}(\omega)d\omega} \tag{4}$$

where $\Omega\in[\omega_L,\omega_H]$, and $\omega_H = 2\pi f_H$ and $\omega_L = 2\pi f_L$ are the upper limit and the lower limit frequencies that limit the operable UWB spectrum, respectively. The magnitude frequency response of the UWB channel (between positions B and C in Fig. 1), normalized to its maximum value over the operable UWB band, is denoted by $|H_{norm}(j\omega)|$; $0 \le |H_{norm}(j\omega)| \le 1$. Accordingly, the RE of gaussian case IR-UWB signal located at the transmitter side, corresponding to position B shown in Fig. 1, is analytically obtained by substituting $|H_{norm}(j\omega)|^2 = 1$ and ((2)) into (4) as follows:

$$\begin{aligned}\eta^k_{g,\text{TX}}(\tau_g) &= \pi(\tau_g A^k_g)^2\int_{\omega_L}^{\omega_H}\omega^k\exp(-(\omega\tau_g)^2)d\omega\\ &= G_p\times(\Xi(\omega_H\tau_g/\sqrt{2}) - \Xi(\omega_L\tau_g/\sqrt{2}))\end{aligned} \tag{5}$$

where $G_p = 2\pi(\tau_g A^k_g)^2(\sqrt{2}/\tau_g)^{k+1}$, A^k_g is the normalization parameter of the *kth* derivative of the gaussian case IR-UWB signal [10] and $\Xi(u)$ is expressed by

$$\begin{aligned}\Xi(u) = {} & (1-s)\Gamma\left(\frac{k+s+1}{2}\right)\operatorname{erf}(u)\\ & - e^{(-u^2)}\sum_{n=0}^{L-1}\frac{\Gamma\left(\frac{k+1}{2}\right)}{\Gamma\left(\frac{k+1}{2}-n\right)}u^{k-2n-1}\end{aligned} \tag{6}$$

where s = remainder$((k+1),2)$, $L = \frac{k+s}{2}$; and both erf(.) and $\Gamma(.)$ are the well-known Gaussian error function and Gamma function, described, respectively, as follows:

$\Gamma(u) = \int_{\zeta=0}^{\infty}\zeta^{u-1}e^{-\zeta}d\zeta$

$\operatorname{erf}(u) = \frac{2}{\sqrt{\pi}}\int_{\zeta=0}^{u}e^{-\zeta^2}d\zeta$

In a similar way, for the sech case IR-UWB signals, the RE before wireless transmission is analytically obtained as follows:

$$\begin{aligned}\eta^k_{s,\text{TX}}(\tau_s) &= 2(A^k_s)^2\int_{\omega_L}^{\omega_H}\omega^k(4\pi\tau_s)^2\operatorname{sech}^2(2\pi\omega\tau_s)d\omega\\ &= S_p\times(\Lambda(2\pi\omega_H\tau_s) - \Lambda(2\pi\omega_L\tau_s))\end{aligned} \tag{7}$$

where $S_p = 8m!(4\pi\tau_s A^m_s)^2(1/2\pi\tau_s)^{m+1}$. A^m_s is the normalization parameter of the kth derivative of a sech case IR-UWB signal and $\Lambda(\zeta)$ is expressed by the following equation

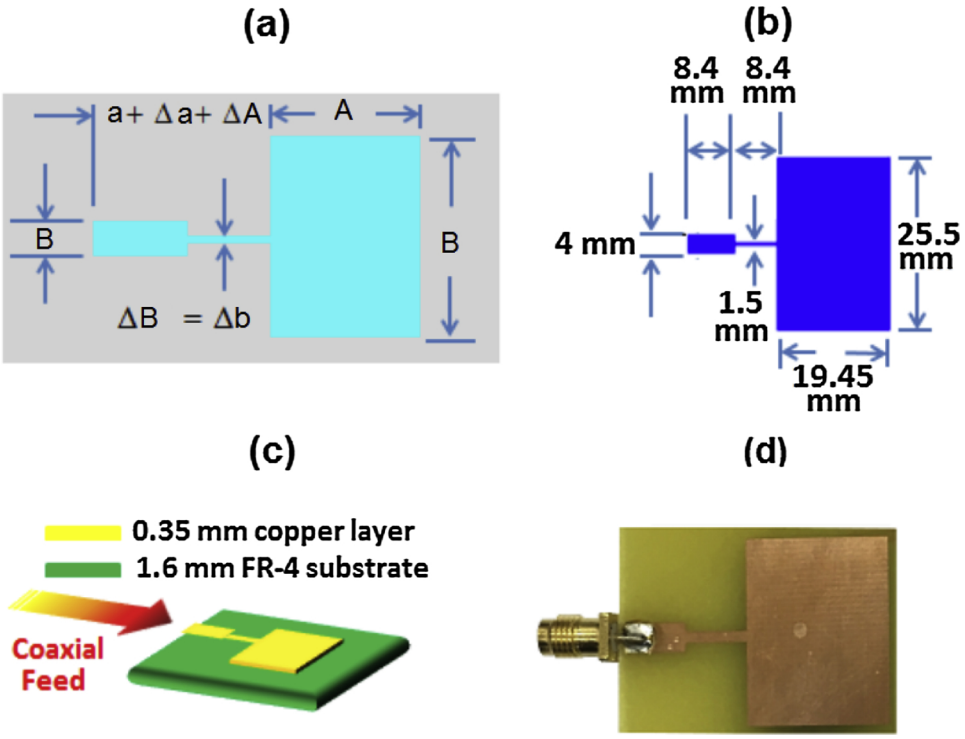

Fig. 2. Design and realization phases of the developed Ultra-Wide Band PMA antenna. (a): Geometrical layout dimensions of the developed Ultra-Wide Band antenna. (b): Selected values for the dimensions of the antenna layout (c): Antenna feed (d):the image for a lab manufactured antenna, both antennas at positions B and C are of similar design.

$$\Lambda(\zeta)= \sum_{i=0}^{T}\sum_{j=0}^{m} \frac{(-1)^{i+j}(i+1)}{(m-j)!(-2(i+1))^{j+1}} \times \zeta^{m-j} e^{(-2i-2)\zeta} \quad \text{where } T \gg 1 \tag{8}$$

To obtain more accurate value for the $\Lambda(\zeta)$ function, the value of T should be increased. The upper limit radiation efficiency for the considered IR-UWB signals can be obtained from Eqs. (5) and (7), regardless of the spatial-spectral specifications for the UWB channel frequency response and the particular designs of the UWB antennas. In practice, the numerical values of $|H_{norm}(j\omega)|^2$ at discrete measurement frequencies is the only available information. Even if $|H_{norm}(j\omega)|^2$ is given analytically, Eq. (4) integrals cannot be easily computed as closed form expression because all of the integrals of products of Gaussian and sech basis signals along with their kth derivatives with other analytical functions are of highly complicated mathematics. Accordingly, the RE at the receiver side, corresponding to position C in Fig. 1, which is numerically evaluated by substituting (2) as well as the measured numerical values of $|H_{norm}(j\omega)|^2$ into (4). The received RE is denoted by $\eta^m_{g,RX}$ and $\eta^m_{s,RX}$ for Gaussian and sech cases IR-UWB signals, respectively.

3. Antenna design, experiment and measurements

The proposed design consists of the discontinuous coupling of a $B \times A\,\text{mm}^2$ radiating element to a $B \times A\,\text{mm}^2$ rectangular microstrip feed line via a $(\Delta A + \Delta a) \times \Delta b\,\text{mm}^2$ strip as illustrated in Fig. 2(a). Only the 2 antennas are tested for s-paramters and their performance in [12]. The proposed design is fabricated using the photolithography technique by depositing a copper layer with a thickness $t = 0.35$ mm on a side with thickness = 1.6 mm of FR-4 dielectric substrate, without ground layer on the opposite side. The FR-4 with a dielectric of relative permittivity of the dielectric equals $\varepsilon_r = 4.4$. The resulting dimensions of the developed design are: $B = 25.5$ mm, $b = 4$ mm, $A = 19.45$ mm, $a = 8.4$ mm, $\Delta A + \Delta a = 8.4$ mm. The entire structure, which resembles a ground-free planar monopole antenna, with an area equals 30 mm × 22 mm and with an excitation source connected to the microstrip feed line then to a conductor with a 50 ohm coaxial cable. Fig. 2(d) shows the image for a lab manufactured antenna, both antennas at positions B and C are of similar design.

The UWB channel frequency response, denoted by $|H(j\omega, L)|^2$; is measured using both fabricated antennas prototypes mounted in the setup shown in Fig. 3(a). Both antennas are mounted in a face aligned organization and along the directions of the peak radiation at a 1100 mm height from the ground, and connecting their feed ports to the vector network analyzer (VNA) terminals through the feeder connectors of two 50 ohm coaxial cables. Throughout the measurement process, both antennas are separated by a distance $L = 30$ cm, then 20 cm and finally 10 cm. To avoid excessive channel losses, such small distances are chosen, this also reduces the

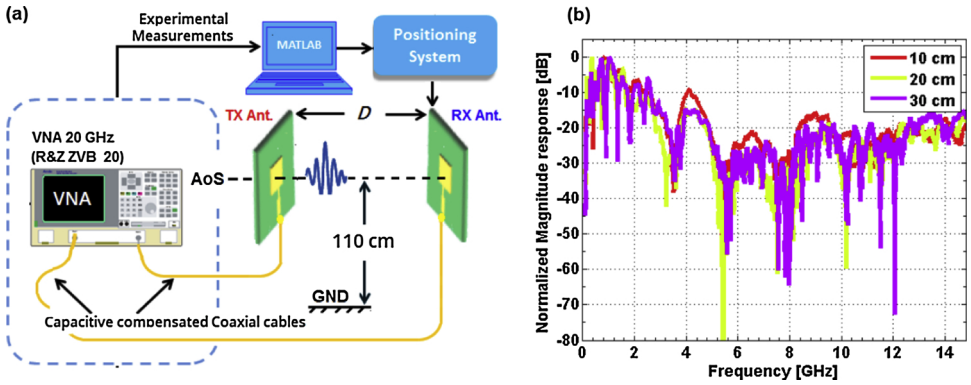

Fig. 3. Full experiment setup and UWB channel frequency response. (a): The details of the experiment. (b): Graph of UWB channel magnitude spectrum at $L = 30$ cm, 20 cm and 10 cm.

need of extra hardware amplifiers needed in case of fading channel effects appears at the receiving antenna. Not only, such small distance helps avoid fading channel losses but also guaranteeing line of sight transmission and reception reducing the impact of multi-path reflections off the walls, windows and any other obstacles that usually residing inside the lab [13].

The Magnitude spectral response is measured at different time instants to guarantee time invariant property, these measurements are done along at all of the different distances using a 20 GHz VNA (ROHDE & SCHWARZ ZVB20) with operating range 10 MHz to 15 GHz, catching 20 k points. Resulted in a resolution bandwidth of the VNA measurements equals 745 kHz, ensuring 1 MHz step obeying the FCC mask regulations [1] and accuracy up to 3 digits after the floating point with GHz frequency measures. Furthermore, the received UWB channel spectrum magnitude is then smoothed using a frequency domain moving average (MA) windowing filter of 10 samples width. Fig. 3(b) plots the measured UWB channel frequency response at the considered TX-RX antenna separation distances. Clearly, in addition to the UWB FCC masking regulations in the frequency domain, the frequency response of the TX antenna – wireless channel – RX antenna chain shows a bandstop filtering effect around 3.5 GHz and 5.5 GHz. These notches impose additional spectral limits on IR-UWB signals represented as occupied bandwidths.

4. Results and discussions

Fig. 4 (a) and (b) illustrate Simulation results of the radiation pattern polar plot in both YoZ and XoZ directions, respectively using the HFSS tool. Simulation is done at the operable Ultra-Wide Band central frequency f_o, such band extends from $f_L = 3.1$ GHz up to $f_H = 10.6$ GHz and $f_o = 0.5 * (f_L + f_H) = 6.85$ GHz. As clear from both figures, the radiation specifications of the developed design are quasi-omnidirectional in both XoZ and the YoZ plans. Obviously, both patterns ensure adequately uniform coverage in typical indoor application scenarios having different TX-RX relative orientations.

Throughout all simulations, the FWHM pulse width τ is tuned from 0 to a maximum value of 500 ps. Trying all of the following derivatives with $k = 1, 2, \ldots, 7$ From [1], $\max\{S_{\mathrm{FCC}}(\omega)\} = -41.3$ dBm/MHz, $f_L = 3100$ MHz and $f_H = 10.6$ GHz. The values of A_n are computed during the simulation in (3) for each signal type and order k. Fig. 5(a) and (b) plot the variations of $\eta^m_{\mathrm{g,TX}}$ and $\eta^m_{\mathrm{g,RX}}$, respectively versus τ for Gaussian case IR-UWB signals, while Fig. 5(c) and (d) depict the variations of $\eta^m_{\mathrm{s,TX}}$ and $\eta^m_{\mathrm{s,RX}}$, against τ for sech case IR-UWB signals. As expected, based on the analytical expressions in (5) and (7), the variation of $\eta^m_{\mathrm{g,RX}}$ and $\eta^m_{\mathrm{s,RX}}$ with τ are always upper bounded by $\eta^m_{\mathrm{g,TX}}$ and $\eta^m_{\mathrm{s,RX}}$, respectively. Due to the inherent frequency-dependent transmission loss exhibited by the UWB channel, including the TX and RX antennas, this observations can be generalized to validate the applicability of the closed-form expressions derived in Section 2 as upper bounds for the RE of IR waveforms emitted by practical arbitrary UWB antennas.

Interestingly, for each UWB signal type and derivative k; find an optimum FWHM pulse width at which the RE attains a global maximum. Moreover, increasing the value of m results in larger better FWHM pulse width value, regardless of the waveform type. It should be highlighted that, the differences between the REs of two corresponding waveforms (i.e., at the same point along the transceiver chain, at the same pulse width τ and order k) derived from the two considered basis functions are not quite significant. However, the RE of a particular sech case pulse is achieved at about half the pulse width of its Gaussian counterpart. A major consequence of this observation is that the rate of UWB signalling using a sech-based IR-UWB waveform is twice as much the rate expected from a Gaussian-based pulse. For example, a Gaussian monocycle pulse shows a maximum RE of about 83% at a FWHM pulse width of about 50.2 ps, while the same RE value is achieved by a sech monocycle at 27.03 ps. Another interesting observation is that, any arbitrary UWB antenna should be fed by a monocycle pulse, derived from either a Gaussian or a sech basis function, if an optimal IR-UWB waveform with a maximum radiation efficiency is desired. The radiation efficiencies resulted from MATLAB simulations for IR-UWB with derivatives upto 7th derivative for both guassian and sech basis function are shown before and after transmission in Fig. 5.

The bit error rate for the complete IR-UWB system [14] utilizing the proposed antenna design is also measured to assesses the communications performance, the BER calculations are done in the MATLAB part of the system shown in Fig. 3(a) where the BER results against different noise power levels are shown in Fig. 6.

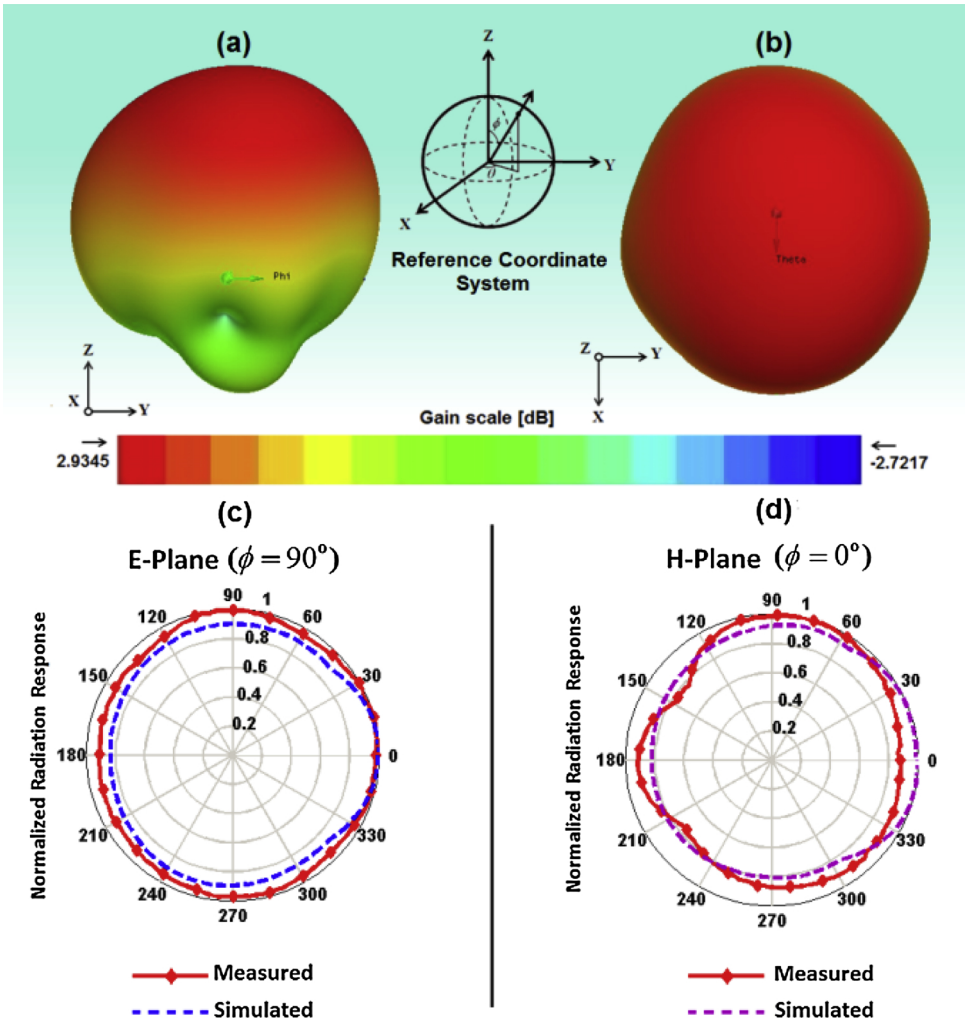

Fig. 4. Radiation Response. (a) E-Plane, (b) H-Plane and the normalized radiation response, (c) E-Plane and (d) H-Plane.

5. Conclusion

In this paper, well-known analytical formulas are developed for the spectral radiation efficiency of UWB waveforms fed to arbitrary UWB antennas. Impulse radio UWB waveforms derived from Gaussian and sech basis functions are considered, and the FCC spectral constraints are placed on their radiated energy spectral densities. Moreover, an UWB antenna is designed, fabricated and its frequency response is experimentally measured. The impact of the UWB channel spectrum, along with the designed antenna, on the spectral radiation efficiency of the considered waveforms is numerically evaluated. It is shown that the derived expressions constitute the upper bounds on the transmit energy and the receive energy of UWB waveforms fed to practical UWB systems.

6. Methods

The radiation patterns of the proposed antenna structure are numerically evaluated using the Finite Element method (FEM), which is adopted by the commercial ANSYS HFSS software simulation platform. Two identical antennas are fabricated, using the photolithography technique, by depositing a 0.35 mm thick copper layer on a 1.6 mm thick FR4 substrate, which have a relative permittivity and a loss tangent of 4.4 and 0.02, respectively. Throughout the experimental measurements, the ultrawide band channel spectrum is measured and recorded using the (R & ZZVB 20) vector network analyzer (VNA).

Conflicts of interest

The authors declare no conflicts of interest.

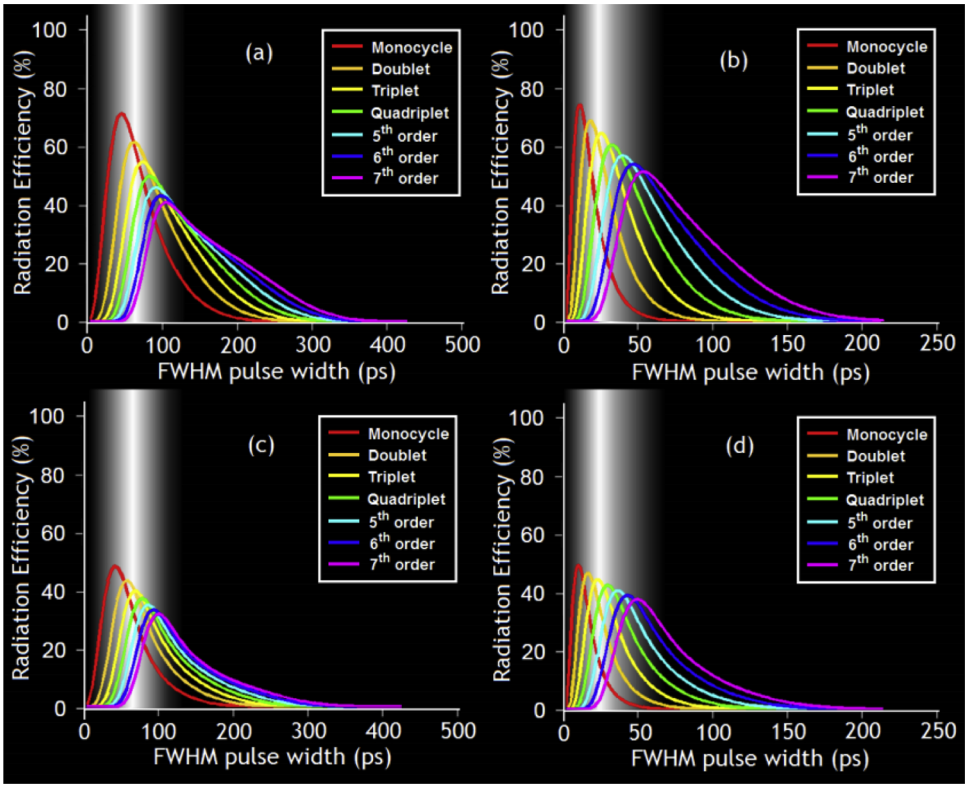

Fig. 5. Radiation efficiency of IR-UWB signals against the FWHM pulse width. Gaussian case signals before wireless transmission. (b): sech-based waveforms before wireless transmission. (c): Gaussian-based waveforms after wireless transmission. (d): sech-based waveforms after wireless transmission.

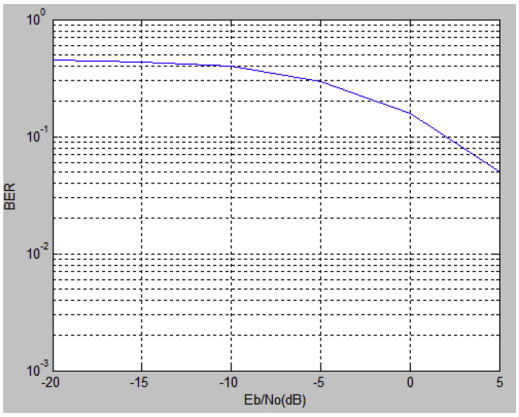

Fig. 6. Bit error rate of the IR-UWB Received signal against different simulated SNR of the communications channel.

Acknowledgements

This project is sponsored and supervised by the National Telecommunications Regulatory Authority of Egypt (NTRA-Egypt). The authors also acknowledges the National Telecommunication Institute (NTI) for providing the required facilities to conduct the experimental measurements.

References

[1] US. Fed. Comm, Commission First Report and Order. Revision of Part 15 of the Commission's Rules Regarding Ultrawideband Transmission Systems. Tech. Rep. (2011).
[2] D.M. Pozar, Closed-form approximations for link loss in a uwb radio system using small antennas, IEEE Trans. Antennas Propag. 51 (2013) 2346–2352.

[3] H. Feng, M.P. Fok, S. Xiao, J. Ge, Q. Zhou, M. Locke, R. Toole, W. Hu, A reconfigurable high-order uwb signal generation scheme using rsoa-mzi structure, IEEE Photonics J. 6 (2014) 1–7.
[4] A. Naji, P. Warr, M. Beach, K. Morris, A fundamental limit on the performance of geometrically-tuned planar resonators, IEEE J. Lightw. Technol. 26 (2008) 628–635.
[5] D.M. Pozar, Waveform optimizations for ultrawideband radio systems, IEEE Trans. Antennas Propag. 51 (2003) 2335–2345.
[6] D.M. Pozar, Optimal radiated waveforms from an arbitrary uwb antenna, IEEE Trans. Antennas Propag. 51 (2007) 3384–3390.
[7] L. Gingras, W. Cui, A.W. Schiff-Kearn, J.-M. Ménard, D.G. Cooke, Active phase control of terahertz pulses using a dynamic waveguide, Optics Express 26 (5) (2018) 13876–13882.
[8] G. Avdeenko, T. Narytnyk, V. Korsun, V. Saiko, Simulation of a terahertz band wireless telecommunication system based on the use of ir-uwb signals, Telecommun. Radio Eng. 78 (2019) 901–919.
[9] M. Shehata, M. Sameh Said, H. Mostafa, A generalized framework for the performance evaluation of microwave photonic assisted ir-uwb waveform generators, IEEE Syst. J. 3 (2019) 1–11.
[10] M. Shehata, M. Sameh Said, H. Mostafa, Photodetected power maximization of photonically generated impulse radio ultrawide band signals, IEEE International Symposium on Circuits and Systems (ISCAS) (2018) 5.
[11] Y. Ismail, M. Shehata, H. Mostafa, On the theoretical limits of the power efficiency of photonically generated ir-uwb waveforms, J. Lightw. Technol. (2018).
[12] H. Mostafa, M. Shehata, M. Sameh Said, A compact uwb antenna design for indoor wireless applications, IEEE 61st International Midwest Symposium on Circuits and Systems (MWSCAS) (2018).
[13] H. Mostafa, M. Shehata, M. Sameh Said, Dual notched band quad-element mimo antenna with multi-tone interference suppression for ir-uwb wireless applications, IEEE Trans. Antennas Propag. (2018).
[14] M. Shehata, H. Mostafa, Y. Ismail, Closed-form expressions and bounds for the signal to noise ratio in ir-uwbof systems, IEEE Photonics Technol. Lett. 29 (2017) 3.